Journal of Power Sources Advances 10 (2021) 100065

Contents lists available at ScienceDirect

Journal of Power Sources Advances

journal homepage: www.sciencedirect.com/journal/journal-of-power-sources-advances

Three-dimensional foam-type current collectors for rechargeable batteries: A short review

Nurbolat Issatayev [a], Arailym Nuspeissova [a,*], Gulnur Kalimuldina [b], Zhumabay Bakenov [a,c,**]

[a] National Laboratory Astana, Nazarbayev University, Kabanbay Batyr Ave. 53, Nur-Sultan, 010000, Kazakhstan
[b] Department of Mechanical and Aerospace Engineering, Nazarbayev University, Kabanbay Batyr Ave. 53, Nur-Sultan, 010000, Kazakhstan
[c] Department of Chemical and Materials Engineering, Nazarbayev University, Kabanbay Batyr Ave. 53, Nur-Sultan, 010000, Kazakhstan

ARTICLE INFO

Keywords:
Current collectors
Foam type current collector
Lithium-ion batteries
Three-dimensional

ABSTRACT

Energy storage systems as lithium-ion batteries (LIBs) have become an essential part of our lives, powering on-the-go technologies we use every day. Until recently, immense attention was paid to designing and synthesizing advanced active materials for LIBs to enhance the battery characteristics. However, not the least crucial part of the battery, the current collector, was left unattended for a long time. Therefore, it is not surprising that the batteries reached their limits in power and energy densities, leaving the battery progress equal to an almost flat line. The only way to go ahead with the battery technology would be to design new architectures or to investigate new materials. Changing the battery current collector from planar to three-dimensional (3D) would offer dimensionality to the electrodes meaning short diffusion length for Li-ions, which will boost power density, more active material, and mechanical stability. Herein, in this review, various 3D architecture current collectors will be summarized, and recent advances in synthesis routes will be discussed to point out the importance of 3D structures. In addition, the correlation between the electrochemical performances of batteries and current collector architecture will be reviewed. More than 50 research publications related to the synthesis and performance of different 3D current collectors were reviewed and compared. The review results suggest that despite the outstanding performance, currently used technologies to obtain 3D current collectors make them unacceptable in the commercial sphere, and cheaper, faster and simple synthesis routes are desired to be explored.

1. Introduction

In recent years, fossil fuel usage has been significantly reduced considering the environmental damage caused by carbon dioxide emissions. Despite this, the energy demand of modern society is increasing at a rapid speed. Therefore, to fill the gap in energy deficiency, environmentally friendly, reliable and, sustainable energy sources should be explored, and devices for storing them should be developed accordingly [1]. So far, different technologies have been developed to store electrical energy as capacitors, fuel cells, batteries, etc. The significant advantages of these systems are long service life, low cost, good cyclability, and portable size [2]. Lithium-ion batteries (LIBs) have been considered one of the most successful technologies to store electrical energy. They are rapidly developing owing to their high energy density, power density, and long life compared to other secondary batteries (Pb-acid, Ni-Cd, Ni-MH) [3].

Nevertheless, LIBs with even higher energy and power densities need to be developed due to the demand for more advanced electronics, hybrid, plug-in and electric vehicles (EVs) [4]. The energy density (the amount of energy stored per unit mass or volume) and power density (maximum practical supported output power per unit mass or volume) are the two critical quality indicators of secondary batteries that need to be enhanced. Energy density is a critical parameter used in almost all energy storage technologies, and it must be high, whereas power density is a key factor for the applications, which require fast charge or discharge. Systems with a high-power density require materials that maintain a high permissible energy transfer rate. These materials and their three-dimensional (3D) spatial arrangement are crucial determinants of energy and power density [7].

In order to enhance the parameters described above battery constituents must be upgraded. Conventional LIBs usually consist of five key components: negative (anode) and positive (cathode) electrodes,

* Corresponding author.
** Corresponding author. National Laboratory Astana, Nazarbayev University, Kabanbay Batyr Ave. 53, Nur-Sultan, 010000, Kazakhstan.
E-mail addresses: arailym.nurpeissova@nu.edu.kz (A. Nuspeissova), zbakenov@nu.edu.kz (Z. Bakenov).

https://doi.org/10.1016/j.powera.2021.100065
Received 15 March 2021; Received in revised form 14 July 2021; Accepted 29 July 2021
Available online 13 August 2021

electrolyte, separator, and casing (cell design). In turn, the electrode contains an active material, a conductive additive, a current collector, and a polymer binder. The chemical nature of active materials used in an anode and cathode determines the energy output. In contrast, an electrolyte in most situations determines how quickly energy can be released by controlling the mass flow rate inside the battery [6]. So far, to increase the efficiency of LIBs, plentiful new electrodes, electrolytes, and separators were investigated. Since the specific energy determines the battery capacity by mass (W kg^{-1}), the energy received from the active material is divided by the entire mass of the battery (conductive additives, binders, current collectors, electrolyte, and packaging). Two ways can achieve energy density increase: 1) by reducing the weight of the inactive components; 2) by increasing the active mass or changing the structure of the active material. Most studies have focused on the latter, which shows that using anode materials with a larger capacity, such as silicon (Si) and germanium (Ge), improves the battery energy density with a specific capacity reaching 3000 mAh g^{-1} for Si. However, the overall increase in battery energy density is usually only about 10 % because of the higher density of Cu current collector and low capacity cathodes [5]. To increase the energy density, a thinner current collector and thicker cathode active material should be used. However, thick cathodes have many problems. Cracks, dropouts, and exfoliation are caused by the volume change in the coated layer during charge and discharge. Besides, the ohmic resistance increases with the increasing thickness of the electrode due to the low electronic conductivity of the composite matrix [5,8].

A current collector is an inactive compartment of a battery connected to an electrode with an external load. Its physical and chemical properties can affect LIB performance [9,10]. Although the current collector has been known as an essential part of the battery performance, the proper insights on the effect of structure, thickness, and material composition are not given due attention [11]. Therefore, the review aims to shed light on 3D current collectors' performance and discuss their latest advances in LIBs. The main attention has been paid to the different preparation methods of foam-type current collectors and their effects on the electrochemical performance of the LIB. This work could help define and understand the most suitable current collector for a particular type of electrodes and battery configurations.

2. Foam-type current collectors

Li ions move from the cathode to the anode during the battery charging operation through the separator and electrolyte [12,13]. When this process occurs, electrons flow through the current collector to the anode, where the reduction reaction occurs with the formation of the Li metal compound. When the discharge occurs, Li ions move from the anode to the cathode in the same way as during the charging process (Fig. 1) [14,15]. The main role of the current collector is to hold the electrode and conduct the electrons through itself, connecting active material and external load. Therefore, the critical criteria for the current collector are high electronic conductivity and sustainability in a particular electrochemical environment. Besides, it does not have to be too thick and heavy so as not to reduce the gravimetric and volumetric energy densities of the system. Moreover, free-standing, mechanically robust, and low-cost current collectors are essential for LIB designs with efficient performance [16].

Current collectors can be classified according to the architecture and constituent materials used as flat and 3D, as well as metallic and non-metallic, respectively. Different metals and their alloys, and non-metallic carbon that meet the above-stated requirements, have been tested as current collectors. In LIBs, various metal foils are usually used as two-dimensional (2D) or planar current collectors. For instance, thin foils of nickel (Ni), copper (Cu), aluminum (Al), platinum (Pt), zinc (Zn), titanium (Ti), and other similar metals have been intensively investigated as a current collector [17]. In the case of all solid-state LIBs, the research on current collector materials is just beginning. The common

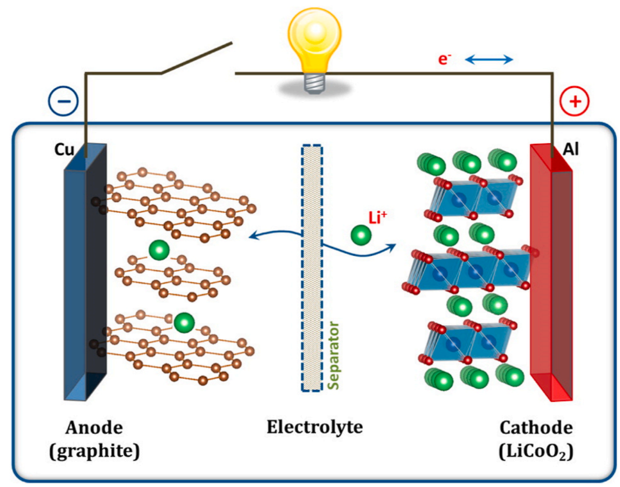

Fig. 1. Schematic illustration of the LIB ($LiCoO_2$/Li^+ electrolyte/graphite). Reproduced with permission [1]. Copyright 2013, American Chemical Society.

current collector materials such as Al, Cu, Ni, stainless steel, and carbon, which do not undergo the reaction with the electrolyte, were simply chosen [18]. Among them, Al and Cu are the most preferred current collectors for cathodes and anodes of LIBs, respectively, owing to their wide stability window in the electrolyte [19].

Moreover, both current collectors have advantages such as lightness, cheapness, good adhesion to the active materials, and good electronic conductivity [20–22]. However, the electrochemical corrosion of Al and Cu still occurs during charge/discharge cycling because of the electrolyte decomposition. The fluorine-based electrolytes, such as lithium hexafluorophosphate ($LiPF_6$) and lithium bis(trifluoromethane sulfonyl) imide (LiTFSI), decompose and generate HF that reacts with the current collectors leading to capacity degradation of the batteries [23]. Also, the small surface area provided by the flat metallic sheets for slurry casting is not favorable. Hence, 3D structures with a hierarchical architecture have attracted immense attention as a type of alternative current collector.

There are many advantages of using 3D materials as a current collector, such as a short diffusion length for Li ions, high electronic conductivity, ability to suppress the growth of Li dendrite, and a large surface area which in turn can help to increase the mass of the active material [24,25]. Metal and carbon materials with diverse architecture can be used to create 3D current collectors. It should be noted that various characteristics of the current collector (pore size, porosity, density, and thickness) could significantly affect and manipulate LIB performance. In turn, the preparation method and the selected conditions affect the architecture of the current collector. Therefore, we concentrated on the 3D current collector preparation methods, described their properties, and the effect on the performance of LIB [26].

3. Preparation methods of 3D foam-type current collectors

The 3D current collector's foam-type structure is recognized as one of the promising, offering high surface area, short diffusion length, and ease in all battery components' integrity. Different methods such as chemical vapor deposition (CVD), electrodeposition, dealloying, and pyrolysis can be used to fabricate technology, as demonstrated in Fig. 2. The next section is devoted to the synthesis methods of 3D materials with various examples and their electrochemical characteristics in LIB.

3.1. Chemical vapor deposition

Foam-type materials, such as Ni, Cu, Al, and carbon (C), found wide application in LIBs as a current collector and an electrode itself. One way

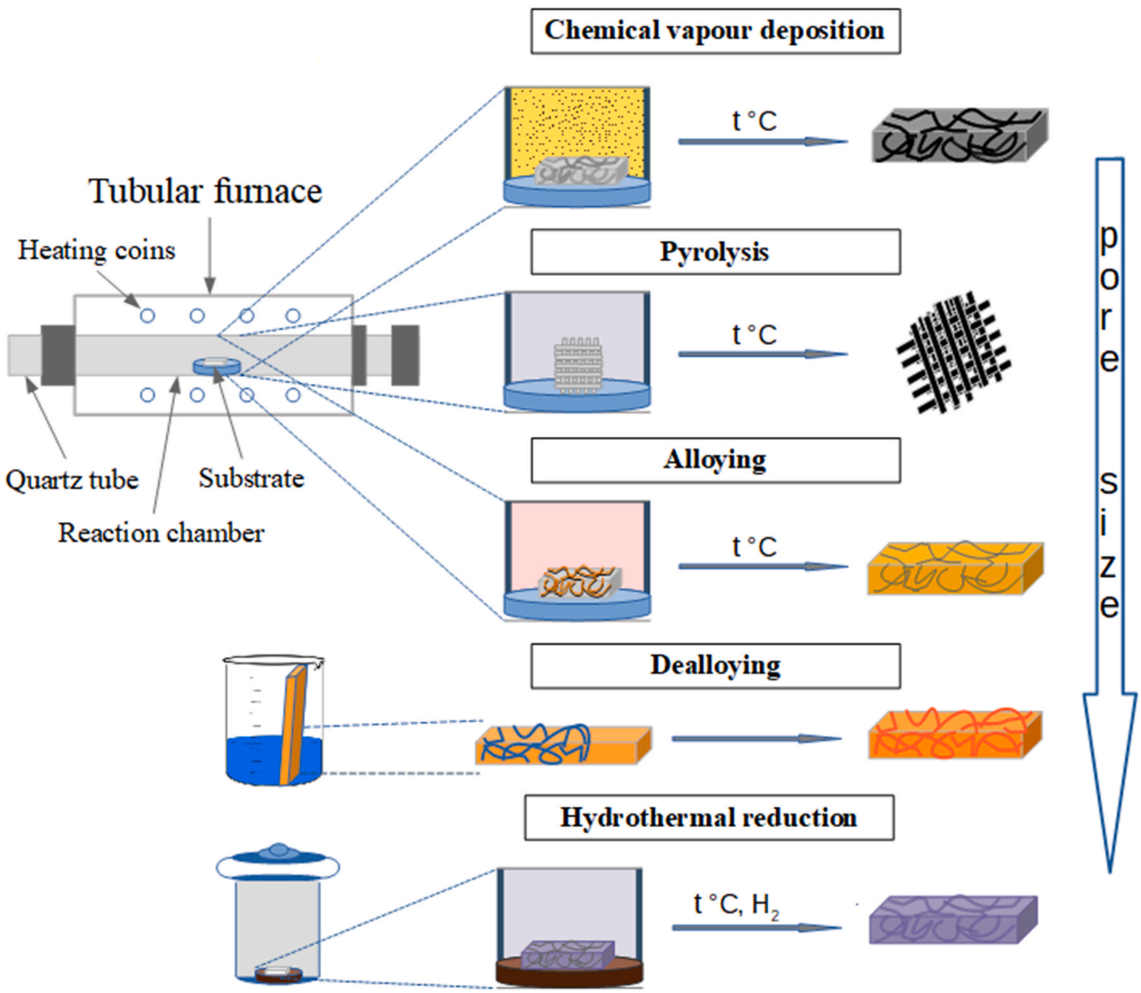

Fig. 2. Visual illustration of the reviewed methods for the preparation of 3D current collectors.

to prepare foam-type materials is by using the CVD technique. The substrate is exposed to volatile gas precursors in a typical process, which react or decompose on the heated substrate surface [27,28]. The Ni foam production involves the deposition of Ni from gaseous nickel carbonyl ($Ni(CO)_4$) onto open-cell polyurethane foam (PU). In detail, PU is placed in a CVD reactor through which gaseous nickel carbonyl is purged using carbon monoxide (CO), which decomposes in the heated reactor (approximately 100 °C) to Ni and CO, and coats PU template. Afterward, Ni-coated PU foam undergoes a PU burnout process, and then the Ni framework is sintered at about 1000 °C to improve the quality of the final product. This method has several advantages, such as 1) one-step Ni plating with the desired density of the material, which can be achieved by adjusting the residence time of the substrate inside the coating chamber; 2) high purity of the resulting material (99.8 % Ni); 3) uniform deposition; 4) controllable pore size in hundred micrometers in diameter, which is determined by the pore size of PU template (Fig. 3a and b); 5) automated process control; 6) the ability to manufacture foams of various densities of stable quality, and 7) the absence of problems with wastewater treatment. However, this method has one significant drawback as the high toxicity of used chemicals [29,30]. Yao et al. reported an investigation of $LiFePO_4$/Cu-Sn LIB, which was constructed with 3D current collectors in both electrodes.

Ni foam was used as a negative electrode current collector; meanwhile, Ni-Cr foam obtained from alloying Ni foam and Cr powder (more details in section 3.5 below) was a positive electrode current collector. Compared to conventional Cu and Al foil current collectors, a battery with a 3D current collector has improved cycle life, maintaining 90 % of the initial battery capacity even at the 200th cycle [31]. Sa and Wang reported incorporating a C-Si electrode into Ni foam, which shows an effective reduction of the electrode expansion and, consequently, a significant in the cycle life of electrodes owing to the network geometry of Ni foam. Electrochemical impedance spectroscopy of the electrode was also examined, which shows a significant decrease in impedance after cycling [32]. Chung and Manthiram reported the examination of Li-S batteries with 3D Ni foam as a cathode current collector. The cathode shows 92 % capacity retention during high capacity discharge, even after 50 cycles (Fig. 3c). Besides, the ability to prevent significant self-discharge was discovered, in which the cathode retains 85 % of the initial capacity after two months. The 3D morphology of Ni-foam helps not only reduces the loss of active material and capacity but also provides an excellent internal electron transport network [33]. Nurpeissova et al. reported another work, where the 3D structure of Ni foam along with the Ni matrix significantly improved the Sn anodes performance [34,35]. Inspired by research mentioned above, Ni foam was used to fabricate various electrodes for LIBs by applying hydrothermal [36–44], chemical bath deposition [45–47], thermal infusion [48], electrostatic spray deposition [49,50], pulse electrodeposition [51], and dip coating [52] techniques.

The CVD technique can also be used to fabricate a monolith of graphene foam (GF). Cheng and his group [53] fabricated GF from the decomposition of methane (CH_4) to C on the surface of Ni foam. The procedure involved the following steps in the CVD reactor, CH_4 is decomposed to graphene (an allotropic form of C) at the temperature of 1000 °C under atmospheric pressure on the surface of Ni foam. It should

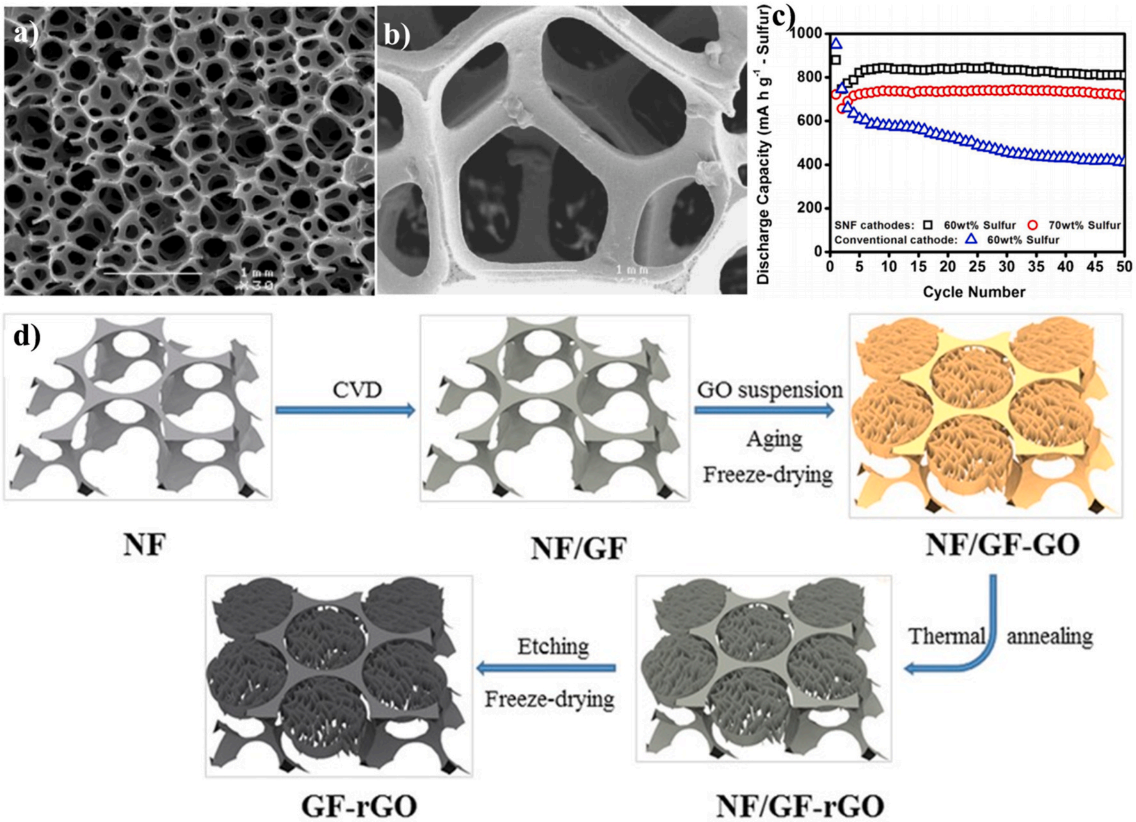

Fig. 3. SEM images of Ni foam at (a) 110 ppi and (b) 20 ppi. Reproduced with permission [30]. Copyright 2004, John Wiley and Sons. (c) Cycling profiles of Li–S cells with the SNF cathodes and conventional cathode at C/5 rate. Reproduced with permission [33]. Copyright 2013, Elsevier. (d) Schematic of the procedure for fabricating 3D GF–rGO hybrid nested hierarchical network macrostructure. Reproduced with permission [55]. Copyright 2015, John Wiley and Sons.

be noted that the Ni template is determined by GF morphology. After cooling down, poly (methyl methacrylate) (PMMA) was deposited on the surface of the obtained product to prevent collapsing of GF's shape during etching away the Ni substrate. Then, Ni foam is etched by a hot solution of hydrochloric acid followed by etching PMMA in hot acetone. The obtained GF demonstrates extreme lightness (~5 mg cm^{-3}) and flexibility, which is essential not only for LIBs but also for all energy storage technologies. Ruof et al. [54] examined the first usage of GF in LIB. The authors synthesized a lithium iron phosphate ($LiFePO_4$) incorporated into ultrathin GF as a cathode in a LIB. The specific capacity of the fabricated electrode was 70 mAh g^{-1} at a charge/discharge current density of 1280 mA g^{-1}. The maximum specific capacity of the cathode (GF loaded with $LiFePO_4$) was 23 and 170 % higher than $LiFePO_4$ coated on either an Al foil or Ni-foam, respectively.

Moreover, it shows an excellent CE of 99.9 %. The lower resistance of electron transfer explained these properties of GF from $LiFePO_4$ to the external circuit and a higher contact surface area of the active material of the electrode with the electrolyte. More works have been motivated to implement such carbon foam (CF) current collectors obtained by the above-mentioned CVD method (**Fig. 3d)** for various electrodes in LIB [55–62]. Furthermore, various companies such as Graphene supermarket have already launched GF on the market. The companies offer various graphene foams such as free-standing GFs, flexible GFs, combined GFs and different metal-based GFs such as Ni, Cu, etc. The method for preparing commercial GF completely coincides with that described above. The average price of a free-standing 3D GF with a size and density of 76.2 mm × 38.1 mm and 85 mg/cm^3, respectively, is 125 $. The high price of graphene foam can be attributed to the use of expensive precursors and high energy consumption during production.

3.2. Electrodeposition

Another efficient method of obtaining a 3D porous framework is electrodeposition. Dehkharghani and Divandari [63] reported the preparation method of Cu foam by electrodeposition technique, which requires five steps starting from 1) cleaning and 2) chemical etching to remove impurities from PU foam; then 3) sensitization and 4) activation to make polymer foam electric conductive as Cu cannot be electroplated directly onto the surface of a non-conductive material; 5) the electroless plating, to produce the foam-type material on the surface of the coated 3D polymer. The PU foam is cleaned out in ethanol in the first two steps, followed by etching by a solution mixture of chromic acid and sulphuric acid. Then follows by the immersing etched PU foam in a sensitization solution of $SnCl_2$ and HCl and then in the activator solution of $AgNO_3$ and HCl, where the attachment of Ag particles to the polymeric substrate occurs by the following reaction:

$$Sn^{2+} + 2Ag^{+} \rightarrow Sn^{4+} + 2Ag \tag{1}$$

Finally, in the last step, the electroplating occurs in an electroplating bath, which has copper sulfate ($CuSO_4{\cdot}5H_2O$) as a source of Cu ions, formaldehyde (HCHO) as reducing agent, ethylenediamine tetraacetic acid (EDTA) as complexant and sodium hydroxide (NaOH) as pH regulator. The process involves the following two half-cell reactions:

Half-cell reaction in the anode

$$2HCHO^{-} + 4OH \rightarrow 2HCOO^{+} + 2H_2O + H_2 + 2e^{-} \tag{2}$$

Half-cell reaction in the cathode

$$Cu^{2+}{}_{(solution)} + 2e^{-} \rightarrow Cu_{(lattice)} \tag{3}$$

Overall reaction is

$$Cu^{2+} + 2HCHO + 4OH^- \rightarrow Cu + 2HCOO + 2H_2O + H_2 \quad (4)$$

The authors found that the optimal parameters for the Cu deposition are the concentration of $CuSO_4$ in the bath for the deposition of 12 g L^{-1}, pH 13, and the temperature range of the electroplated coating 55–60 °C.

Another electrodeposition technique for producing a porous skeleton was proposed by Shin et al. [64]. Typically, the production of dense metal electrodeposition processes can be used, where the accompanying hydrogen development is intentionally suppressed. However, the authors proposed the process of hydrogen bubbles that were used as a dynamic template for metal deposition to obtain 3D foams structures. In the process, Cu and Pt were used as the cathode, and the anode, respectively, and the solution in the electroplating bath contained CH_3COOH (an additive that suppresses bubble coalescence), $CuSO_4$ and H_2SO_4. The distance between the anode and cathode was maintained at 2 cm. Sun et al. obtained porous Cu foam using a similar method with few modifications to implement it as a current collector for Sn–Co alloy negative electrode. To evaluate the electrochemical performance of the obtained current collector, half-cell, coin-type (CR2025) cells were assembled with Li foil as a counter and reference electrode. However, the same coin cell with a 2D current collector (Cu sheet) was assembled for comparison. The Cu@Sn–Co electrode showed the first discharge and charging capacities of 726 and 563 mAh g^{-1}, respectively. The capacity retention was at 71 %, which was 3 times higher than that of the Sn-Co alloy anode with a 2D current collector [65]. More studies using binder-free Cu foam current collectors were reported by the methods of electrodeposition [66], electrochemical oxidation [67], anodization [68], solvothermal [69–73], and others.

3.3. Dealloying

Although above, we highlighted the excellent properties of foam-type current collectors obtained by CVD and electrodeposition, some issues still need to be addressed. One of the drawbacks of these methods is the requirement for using commercially available templates to synthesize foam-type structures. Moreover, the electrical conductivity could be altered negatively due to the poor contact between the active materials and the foam-type current collector. For instance, large pore sizes (hundreds of microns) of foam-type structures deposited on the commercial templates could interfere with creating a tight contact surface area [74]. Yang et al. demonstrated that the Coulombic efficiency (CE) of a commercially available Cu foam decreased to 90 % after 29 cycles, which is worse than that of Cu foil. The reason for the poor performance has been defined as coming through a large amount of deposited Li into the Cu foam, which cannot be stripped entirely to complete the reversible process. The formation of a dead Li on a Cu foam

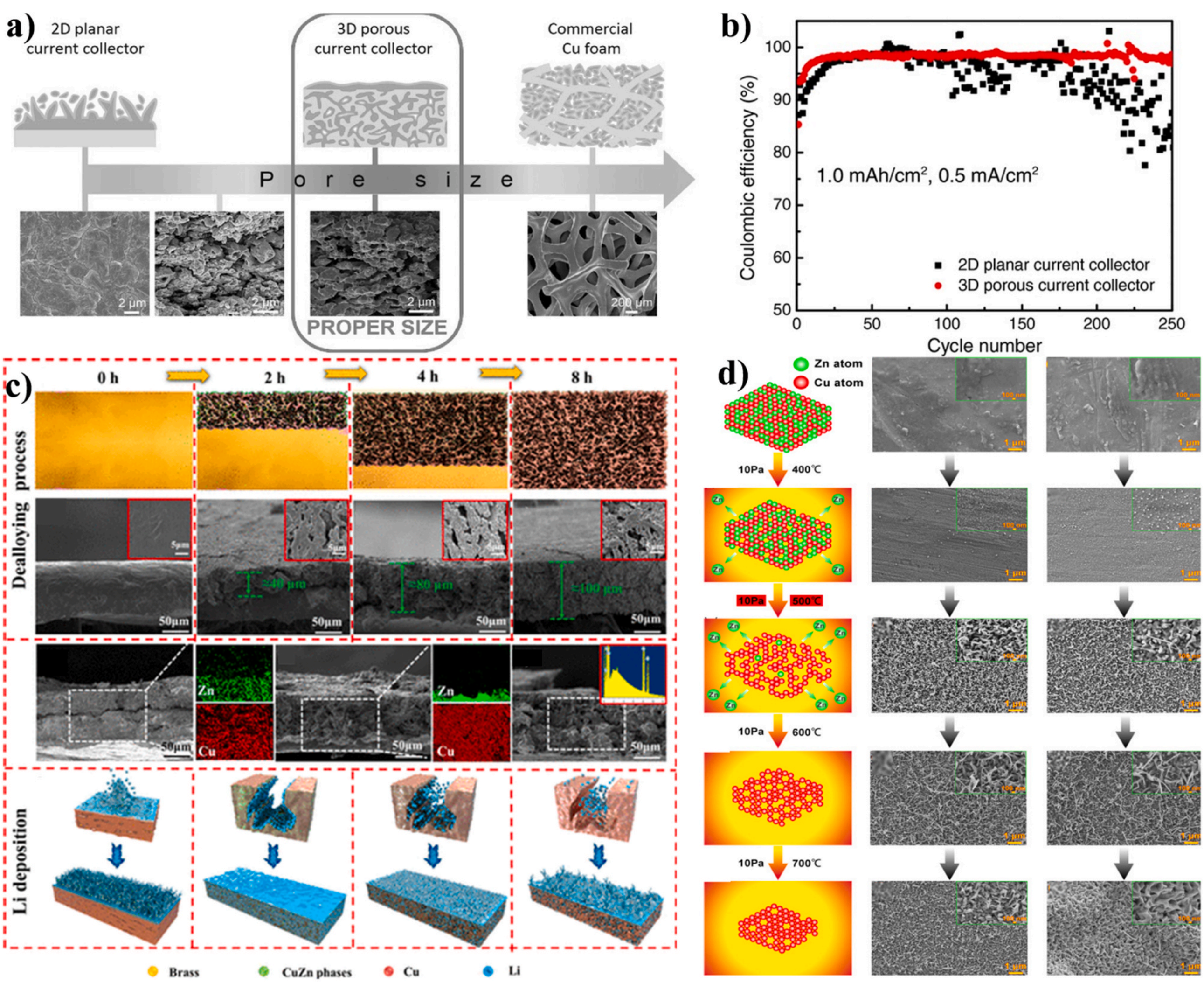

Fig. 4. (a) Principle of designing the 3D current collector for Li metal anode. (b) CE of Li deposition on 2D planar and 3D porous current collectors with current densities of 0.5 mA cm^{-2}. a,b) Reproduced with permission [25]. Copyright 2016, John Wiley and Sons. Scheme of the evolution brass alloy structure treated by (c) chemical dealloying method and (d) physical dealloying method, with SEM images of the evolution structure of the dealloyed brass alloy. c) Reproduced with permission [78]. Copyright 2020, American Chemical Society. d) Reproduced with permission [82]. Copyright 2018, Elsevier.

structure promotes low CE. To avoid the problems of large pore size 3D current collectors, a dealloying method has been investigated as an alternative method to fabricate porous current collectors (Fig. 4a) [25]. Dealloying is the selective "splitting" of the metals based on their differences in chemical, electrochemical, and physical properties [41,75]. This process leads to the formation of nanoporous foams, consisting of nobler alloy components. There are three routes for the dealloying approach: chemical, electrochemical, and physical.

Chemical Dealloying. Chemical dealloying is an artificially induced corrosion process by chemical substances such as acids, base, and others of a less noble element in the alloy to form a uniform porous architecture [76]. Yang and co-workers reported the fabrication of porous Cu from a commercially available Cu-Zn alloy by dissolving Zn in HCl and NH_4Cl mixture solution. The obtained porous Cu had pore sizes varying from ~200 nm to ~2 μm, easily controlled by the dealloying time. After that, it was directly used as a current collector for Li anode. To test the properties of an anode, the full-cell was assembled with $LiFePO_4$ cathode (porous Cu/Li || $LiFePO_4$). Compared to the 2D current collector typically used for Li anode, the obtained 3D Cu current collector demonstrated a significant improvement in cycling performance. The reversible capacity was 136 mAh g^{-1} after 300 cycles with a CE of 99.7 % and capacity retention of 89.7 %. On the other hand, the 2D current collector exhibited 87.3 mAh g^{-1} with a lower capacity retention of 58.2 % [25].

Zhang et al. prepared a Cu-Ga alloy for the fabrication of 3D nanoporous Cu by the dealloying method. A heated commercially available Cu foil was painted with liquid Ga at 80 °C. Afterward, the obtained alloy underwent a dealloying process in a mixture of HNO_3 and HF. To explore the properties of a 3D Cu, it was applied as a current collector for lithium metal anode and Li@3D-Cu||$LiFePO_4$ full-cells were fabricated. To demonstrate the advantage of such cells, 2D Cu current collector was also used to make cells with $LiFePO_4$ cathode. The cells with 3D and 2D current collectors showed almost the same capacity of 137.5 and 136.3 mAh g^{-1} at the first cycle, respectively. However, the capacity retention of the cell with a 3D current collector was higher at about 80 after 150 cycles. While cells with 2D structured Cu current collectors could reach only 58 %. Moreover, the CE results were collected as 98 % for a 3D current collector, while large fluctuations were observed for the 2D current collector (Fig. 4b) [77].

The superior results obtained by a 3D current collector could come from the nanoporous structure where the initially deposited Li is homogeneously scattered, which leads to the numerous charge centers. Consequently, the electric field becomes uniform that partially prevents the spread of Li dendrites [77]. If we compare such arrangements in 2D Cu current collectors, it has been reported that more Li dendrites have been formed on the surface due to their inhomogeneous deposition. The inhomogeneous deposition is explained by the fact that the initial nucleation of Li is sporadic, and the formed nuclei have a strong electric field, which prevents nucleation at the site of the initial nucleation.

Tang and his research team reported the preparation of 3D-CuZn and 3D Cu current collectors from a commercially available brass sheet (H62, 38 wt% Zn) by dissolving it in hydrochloric acid for a different time (2, 4 and 8 h). Complete removal of zinc from brass occurred after 8 h. The pore size of the obtained porous skeleton ranged from 2 to 8 μm with thicknesses of about 40, 80, and 100 μm for 2 h-3D CuZn, 4 h-3D CuZn and 8 h-3D Cu, respectively (Fig. 4c). To evaluate the electrochemical properties of t3he obtained current collectors, CR2025 coin cells with 3D porous current collectors as « Li-free » working electrodes and Li metal as counter/reference electrodes were assembled. The electrolyte used was 1 M $LiPF_6$ in a mixture of ethylene carbonate (EC) and diethyl carbonate (DEC) with a volume ratio of 1: 1 with the electrolyte additive of 0.1 M $LiNO_3$. After 60 cycles, it was noted that the deposition of Li occurs preferably in the internal pores. After filling the internal pores, Li began depositing on the external pores, which led to the growth of Li dendrites. Obviously, the thinner the current collector, the faster the pores are filled with Li. After 100 cycles, coarse Li dendrites appeared on the thinnest 3D collector (8 h-3D Cu). While 2 h-3D CuZn current collector exhibited excellent cycling stability, long cycle life (1000 h at 0.5 mA cm^{-2} or 450 h at 1 mA cm^{-2}) and a high CE (>95 %) after 220 and 150 cycles at 0.5 and 1 mA cm^{-2}, respectively. The enhanced electrochemical properties of a prepared 2 h-3D CuZn current collector have been explained from numerous nucleation sites that stimulate Li's deposition into the internal pores [78]. In other studies, binder-free electrodes for LIB were also fabricated using a Cu current collector obtained by dealloying and electroplated with tin [79,80].

Electrochemical Dealloying. The electrochemical dealloying process has been considered one of the promising ways to obtain a homogeneous nanoporous morphology. Electrochemical dealloying can be achieved by immersing the alloy in an electrolyte under the action of a driving force. Consequently, the non-reactive components remain in a metallic form, while reactive ones dissolve. In this case, an applied potential or electrolyte can be a driving force. To use the electrochemical dealloying method on alloys, two criteria have to be followed: 1) the complete solubility of alloy components (except for the desired non-reactive components) in the electrolyte; 2) selectively remove one or more components, the metal oxidation potentials must be different. For example, we can take Mn-Cu alloy, where Cu is the inactive component and Mn is the reactive one [81]. However, to the best of our knowledge, nanoporous materials obtained by electrochemical dealloying have not been applied in LIBs yet.

Physical Vacuum Dealloying. Until recently, methods of chemical and electrochemical dealloying were used widely for 3D structures preparation. However, not long ago, Yang and co-workers reported on a new method of physical dealloying. The concept of the novel method lies in the sublimation and Kirkendall voids, where deallying is achieved by applying high vapor pressure on one or more metal components to form the porous metal. To form the metal's pore structures, the temperature has to be below the melting point of the precursor alloy, whereas the evaporation temperature should be above the melting point of the alloy. The advantage of using physical vapor dealloying is in the possibility of obtaining the microporous material (from 0.5 μm up to 10 μm), which cannot be obtained by the traditional preparation method (Fig. 4d) [82]. Liu et al. fabricated $Cu_{30}Zn_{70}$ alloy by heat treatment to use it as a precursor for producing 3D nanoporous Cu by physical dealloying. The treatment of $Cu_{30}Zn_{70}$ obtained the nanoporous Cu matrix with pore sizes from ~0.5 μm to 3.5 μm in a high vacuum at 450 °C. The pore of the obtained porous Cu matrix would act as "cages" for "hostless" Li metal during electrodeposition. The obtained Cu matrix was then immersed in a mixed solution of NaOH and $(NH_4)_2S_2O_8$ to obtain additional nanometer-sized pores (about 200 nm), leading to uniform deposition of Li due to a decrease in the local current density along the surface of the porous Cu current collector. Finally, Cu nanoporous was reduced at 400 °C for 10 h in an H_2/Ar gas mixture to obtain the final product. To evaluate the electrochemical properties of the prepared nanoporous Cu, an R-2032 cell was assembled, in which a 3D Cu current collector was used as a «Li-free » working electrode and a Li foil as a counter/reference electrode. 1 M LiTFSI in a 1: 1 mixture of 1,3-dioxolane (DOL) and 1, 2-dimethoxyethane (DME) solvents with 2 wt% $LiNO_3$ was used as the electrolyte. Nanoporous 3D current collectors showed a high and stable CE of about 98 % over 200 cycles. The unique 3D Cu architecture facilitated the bulk expansion of Li metal during the deposition/dissolution process and inhibited the growth of Li dendrites and mossy Li [83]. Qian et al. used a commercial brass plate (contains 75 % Cu and 25 % Zn) to fabricate a 3D porous Cu current collector. Only a high vacuum, along with various temperatures, was applied to the $Cu_{75}Zn_{25}$ to obtain a porous current collector. The electrochemical testing was performed on 2016-coin cells assembled from a 3D porous Cu current collector as a «Li-free » working electrode, the Li foil as a counter/reference electrode. The electrolyte was 1 M LiPF6 in EC: DEC co-solvent (1: 1). The cell exhibited a stable CE at 0.52 mA $cm^{-2}$and 1.04 mA cm^{-2} after 120 cycles and more than 80 cycles, respectively, significantly reducing polarization. The long battery life of 800 h is achieved in symmetrical Li|Li@Cu cells [82].

3.4. Hydrothermal reduction method

The dealloying synthesis process described above requires a large amount of time and energy. Therefore, the more facile and inexpensive method is necessary for the large-scale production of nanoporous metals for LIBs. As an alternative method for the preparation of current collectors, Pei and colleagues suggested a new template-free, fast, and facile synthesis route [84]. The concept of this method for obtaining a 3D nanoporous structure is based on the thermal decomposition and hydrogen reduction of metal salts and the subsequent rearrangement and growth of particles of the reduced metal (Fig. 5a). This method is considered unique since only hydrogen is needed as a reducing agent and metal salts to provide the metal. To be more precise, water molecules would be removed from nickel nitrate hexahydrate ($Ni(NO_3)_2{\cdot}6H_2O$) by heating. After that, the salt is heated at a temperature of 250–800 °C to obtain a nickel oxide framework and then reduce nickel oxide to Ni with H_2. The overall reaction to the production of nanoporous Ni can be summarized as follows:

$$Ni(NO_3)_2{\cdot}6H_2O_{(s)} + H_{2(g)} \rightarrow Ni_{(s)} + 7H_2O_{(g)} + N_2O_{5\ (g)} \tag{5}$$

The obtained framework had the pore sizes and the ligament thickness ranging from 25 to 600 nm, and 100–200 nm, respectively (Fig. 5b). The joints connecting the ligaments have a length of 600–800 nm. The constructed 3D Ni-skeleton had a much lower density (~ 5.0 g cm^{-3}) than current collectors made of Cu foil (8.96 g cm^{-3}), respectively. It should be noted that not only pristine nanoporous metal can be obtained, but also alloys. The authors prepared a nanoporous NiCo alloy using the same procedure to prove the effectiveness of the method for the alloys.

Electrochemical performances of obtained 3D Ni were evaluated through assembling $NiC_2O_4{\cdot}2H_2O$@nanoporous-Ni binder-free electrode. It was a working electrode; meanwhile, Li metal was used as a counter/reference electrode in the assembled Swagelok type cell. The first discharge achieved a high specific capacity of 3154 mAh g^{-1} and during charge 1910 mAh g^{-1} (Fig. 5c), respectively. The exhibited capacity values were much higher than in the other evaluated oxalates anodes and SnO_2/nanoporous Cu, MnO_2/nanoporous Cu systems using as-prepared $NiC_2O_4{\cdot}2H_2O$@nanoporous-Ni. Compared to $NiC_2O_4{\cdot}2H_2O$@Ni-commercial foam, the $NiC_2O_4{\cdot}2H_2O$@nanoporous-Ni electrode showed a good CE of 60.5 % for the first cycle and 93.5 % for the 30th, while $NiC_2O_4{\cdot}2H_2O$@Ni-commercial foam reached 56.8 % for the first cycle and only 70–80 % for the remaining cycles. So far, scarce works have been reported on the described method, although this approach shows promising outcomes with enhanced electrochemical performances.

3.5. Alloying method

Typically, this method is used to increase the resistance of a 3D metal current collector to corrosion by alloying an additional element into its structure. Ni foam is suitable as a current collector on the anode side, but it goes through corrosion when applied on the cathode side. Therefore, Yao et al. [85] first introduced the method of alloying 3D Ni foam using heating with chromium (Cr) powder. The 3D structured alloy foam's electrochemical tests show a small anode peak at about 4.7 V during the first cycle. The absence of a peak after the remaining cycles in the cyclic voltammetry (CV) curve between 2.0 and 5.0 V was explained by forming a passivation film.

In contrast, pristine Ni foam demonstrates a growing current curve at about 4.0 V due to corrosion. The electrochemical properties of the obtained Ni-Cr alloy were studied with the cathode of $LiFePO_4$ and the anode of Li metal. A cell with an Al foil as a cathode current collector was also constructed to compare the electrochemical performance. The discharge capacity of both prepared cells shows a comparable value for the actual $LiFePO_4$ capacity of about 150 mAh g^{-1}. However, compared with conventional current collectors, the prepared 3D Ni-Cr alloy demonstrated stable charge-discharge characteristics because of the enhanced corrosion resistance. Inspired by this research, Joo et al. carried out different studies to enhance the properties of Ni foam [26, 86–89]. The fabricated NiCrAl alloy foam was used as a current collector for the cathode electrode of $LiFePO_4$/C. According to the authors' works, the thickness of the alloy foam current collector played a significant role

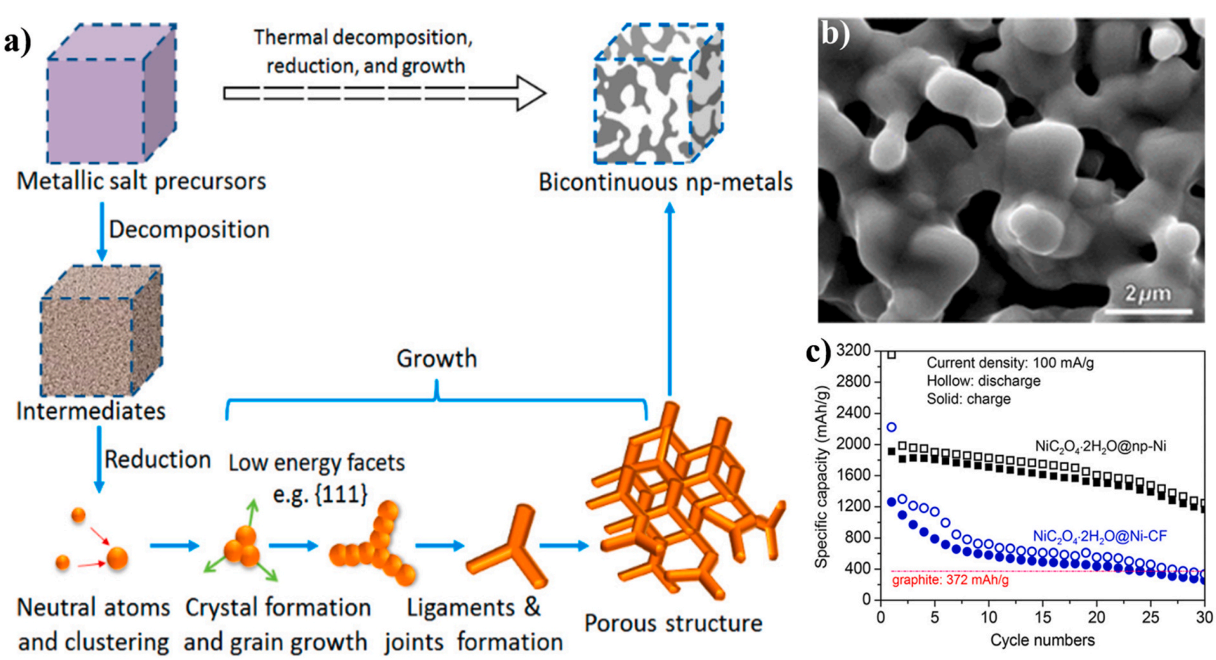

Fig. 5. (a) Schematic illustration of the formation process of nanoporous metals from salts by the method of thermal decomposition, reduction, and growth. (b) SEM images of nanoporous Ni prepared at 600 °C. (c) The cycling performances of $NiC_2O_4{\cdot}2H_2O$@np-Ni and $NiC_2O_4{\cdot}2H_2O$@Ni-CF at 100 mA g^{-2}. a-c) Reproduced with permission [84]. Copyright 2018, American Chemical Society.

in the electrochemical output of the cathode.

3.6. Pyrolysis preparation method

The concept of this method is to burn out a 3D structural C precursor, which preserves the structure and, as a result, gives a 3D C current collector. The C current collectors fabricated by pyrolysis could be categorized as CF, carbon fiber, and carbon paper (CP). The preparation methods will be discussed in the following section.

Carbon foam. CF can be obtained by annealing commercially available polymer foam, as was demonstrated in Fig. 6a [90,91]. Yang et al. used PU foam as a C source and then proceeded with the pyrolysis process under an argon atmosphere at 800 °C to obtain a C current collector for Li-S battery [90]. This study was proposed to prevent environmental pollution and obtain economic and social benefits by recycling PU foam waste. PU foam is widely used in daily life (an estimated 5 % of the total global consumption of plastics). Direct pyrolysis of the wasted polymer, which can later be used as a current collector, solves the global waste problem and can be an inexpensive and straightforward approach to the large-scale production of a current collector. The resulting N-doped CF (NCF) exhibits high porosity of 80 %, elasticity, preferred compressibility, and low density of 0.4 g cm^{-1}. The prepared cells from the PU foam current collector with sulfur cathode showed a large reversible capacity of 1124 mAh g^{-1} at 0.5 C. A high specific capacity of 902.8 mAh g^{-1} has maintained over 100 cycles with a CE of 98.6 % in all cycles. The melamine foam [91], emulsion polymer foam [92], melamine formaldehyde foam [93] were also examined as a C source to obtain CF current collector with promising electrochemical properties.

Carbon fiber. Fibers with a C content at 90 % or higher can be defined as carbon fibers [94]. In preparation, the organic precursor is first spun to obtain an organic fiber-containing several thousand filaments with a diameter of 5–10 μm, and then a series of preliminary oxidation, carbonization, and surface treatment is carried out. Many works are currently reported using carbon fibers based on polyacrylonitrile (PAN), resin, and viscose as raw materials [95]. Carbon fiber has properties such as high tensile strength, high heat resistance, high chemical resistance, fatigue and creep resistance, electrical conductivity and thermal conductivity, low density, high rigidity and lightweight, making it an ideal candidate as a current collector [96,97].

Recently, researchers fabricated a carbon nanofiber current collector for a sulfur cathode as well. The fiber was first obtained by electrospinning of PAN, followed by a heat treatment at 280 °C to stabilize the fiber, and follow up carbonization at 800 °C (Fig. 6b). The cathode was prepared by applying slurry onto the current collector using the vacuum infiltration technique. The slurry consisted of 80 % specially prepared active composite material, 10 % acetylene black (AB) and 10 % PVDF binder. To obtain a sulfur-containing active mass, so-called sulfur/dehydrogenated polyacrylonitrile/multilayer carbon nanotubes (S/DPAN/CNT) composition, sulfur with PAN and CNT was grinded and then heat-treated at 300 °C for 4 h. The electrochemical characteristics of the prepared cathode were evaluated by assembling 2032-coin type half-cells with flat lithium foil as counter and reference electrode. The prepared cell showed an initial specific capacity of 1620 mAh g^{-1} and retained a reversible capacity of 1104 mAh g^{-1} for 100 cycles (Fig. 6c). Besides, the areal density of the nanofiber current collector (0.85 mg cm^{-1}) was almost 10 times lower than that of the commercial Al current collector (7.33 mg cm^{-1}), respectively [98]. More works showed the advantages of using nanofiber current collectors for electrodes in LIBs [99–102]. However, although a carbon fiber-type current collector shows good results, it has disadvantages as the time-consuming synthesis and residual impurity components [103].

Carbon paper. By applying the pyrolysis technique, CP can also be prepared, which has a desirable 3D structure. Zhang and co-workers [104] used the filter paper that is inexpensive and widely available as a precursor of CP. The annealing was used to etch filter paper at 800 °C

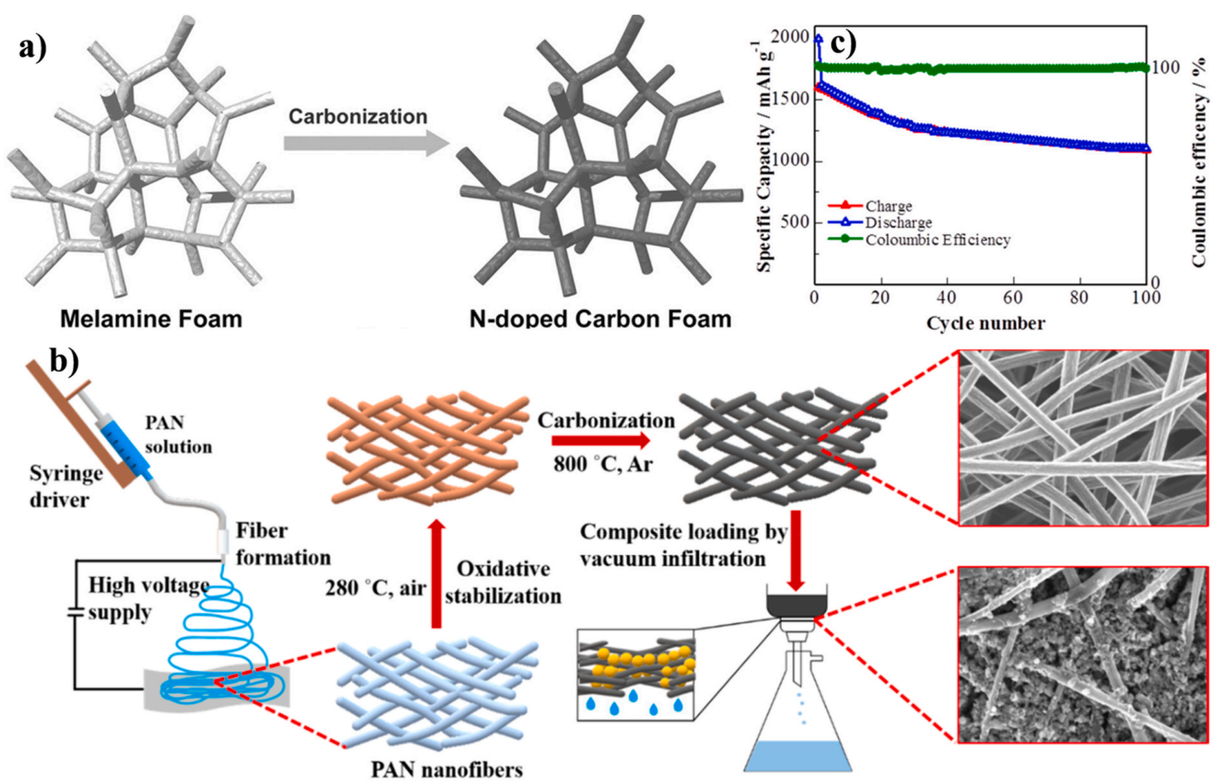

Fig. 6. (a)Schematic diagram of the synthesis of flexible and free-standing nitrogen-doped carbon foam (modified). Reproduced with permission [91]. Copyright 2016, John Wiley and Sons. (b) Cycle performance of the sulfur composite on cPAN CNFs at 0.1C. (c) Scheme of carbon nanofiber fabrication and sulfur-based cathode preparation. b,c) Reproduced with permission [98]. Copyright 2020, MDPI.

under an inert atmosphere. Electrochemical performance testing was carried out by using CR2025-type coin cells with CP@TiO2-S cathode and Li anode. The CP@TiO_2-S cathode showed a good reversible discharge capacity and a high specific capacity of 850 mAh g^{-1} after 200 cycles at a current rate of 0.5 C and 660 mAh g^{-1} at 5 C, respectively. Si et al. [105] used a non-woven cloth made from natural cellulose fiber to produce CP. The electrode of Si/C was loaded onto a prepared current collector. As a result, the electrode exhibited a stable reversible capacity of 1200 mAh g^{-1} after 100 cycles and an initial CE of 90 %.

The demonstrated Table 1 summarizes reported 3D current collectors. From the analysis, we can define the type of electrodes, synthesis methods, and the kind of electrochemical properties that could be achieved using a particular type of current collector.

4. Conclusions and outlook

Although the current collector plays a vital role in rechargeable battery performance and charge-discharge mechanism, the attention on its actual influence has not been properly addressed. Therefore, 3D foam-type current collectors were comprehensively discussed and summarized in this review work. To be successfully applied as a current collector in a LIB, the material should meet the following criteria: high electronic conductivity, stability, lightness, ability to stand freely, mechanical robustness, and cheapness. It can be classified as planar and 3D structured and can be made from metallic and carbon materials. Some advantages of a 3D structure current collector can be highlighted as:

- larger surface area because of its skeleton;
- shorter Li-ion diffusion length due to the many triple points (3D current collector frame, active material, and electrolyte compounds) inside the electrode, which also improves electrical conductivity;
- higher loading mass of the active material, which makes it possible to reduce the mass and the volume of inactive materials;
- bifunctionality of porous materials, acting as a current collector and a unit for active material, can vastly enhance the gravimetric and volumetric capacitance of the electrodes due to their lightness.

These properties make the 3D foam-type current collectors ideal for building flexible electrodes, all-solid-state batteries, and microbatteries. Therefore, we have examined reported works on 3D current collector preparation methods as CVD, electrodeposition, alloying, dealloying, pyrolysis, and hydrothermal reduction. Considering cost, possible scalability the preparation methods and compatibility with cell chemistry the reviewed preparation methods can be ranked as follows:

1. Pyrolysis. The concept of this method is annealing commercially available polymer foam or constructed architecture of a 3D carbon precursor. The most intriguing example is the fabrication of carbon foam from wasted PU foam. This method not only prevents environmental pollution but also provides a facile and low-cost approach to the manufacture of current collector. The inexpensiveness of the synthesis process can be explained by only using an inert gas and energy consumption in order to obtain 3D carbonaceous material. In addition, the widespread use of polyurethane foam in everyday life makes this synthesis process scalable. Moreover, owing to the high electrochemical stability of carbon, three-dimensional carbons can be used as a current collector for both positive and negative electrodes.
2. The hydrothermal reduction method. This method involves obtaining a three-dimensional nanoporous structure by thermal decomposition and reduction of metal salts with hydrogen, followed by rearrangement and growth of the reduced metal particles. This method is easy, fast, and without templates that only require metal salts as metal precursors and hydrogen as a reducing gas. All this would make this method inexpensive. The Ni nanoporous foam is stable only on the anode side, but this method can produce nanoporous alloy and other pure metallic material. However, byproducts such as N_2O_5 may hinder the scaling up of this process due to its high corrosiveness.
3. Electrodeposition. This method is based on metal electroplating on a 3D template. Although a platinum anode is used during production, the process can be inexpensive as it does not consume Pt during synthesis and uses relatively cheap chemicals.
4. CVD. This method allows the fabrication of metallic and carbon foam-type current collectors with hundreds of microns pore sizes. Ni foam and GF have already been commercialized. The reason for this may be due to the fact that this method has several privileges of 1) the desired density; 2) high purity of the resulting current collector; 3) even deposition; 4) tunable pore size in hundred micrometers in diameter. However, the high toxicity of the chemicals used and the need for additional materials, templates, such as commercial Ni or PU foams, make it expensive.
5. Alloying. The alloying approach for fabricating 3D foam current collectors is intended to increase the electrochemical stability of the current collector by doping an additional one or more elements into the metal foam. The advantage of this method is the high stability of the current collector, which gives prolonged battery life. The process may be expensive owing to the requirement of prepared foam materials. The simplicity of the method makes it feasible for commercial production.
6. Dealloying. The concept of the method is an artificially induced process of dealloying by chemicals, physical conditions, or an electrochemical reaction to form a homogeneous porous structure. Various metallic current collectors with smaller pores and excellent quality foam materials could be obtained. However, nanoporous materials manufacture has significantly increased costs due to the lengthy and complicated processes of dealloying. It also requires specially prepared alloys with alloying elements in a solid solution. In addition, the etching time can become quite large, especially for bulk alloys, due to the resistance of bulk diffusion of ions. Moreover, etchants and oxides can be introduced as impurities into the porous structure from the etching process. All this creates an obstacle to industrial production.

The resulting foam current collectors have a different morphology depending on the preparation method, affecting battery performance, and each of them offers meaningful improvement.

Even though 3D current collectors are considered the next technology to improve the battery characteristics, several problems that need to be tackled still remain. Side reactions stemming from a high electrode/electrolyte interface area which results in a low Coulombic efficiency is one of the main concerns. Also, the porous structure of the 3D current collector with its disordered microstructures and low packing density, which causes an increased volumetric density, is recognized as undesirable for battery applications. It is also worth mentioning integrating active materials into a 3D structured current collector which again poses some obstacles. Usually in traditional batteries, the active materials are coated on metal foils easily, however, for a 3D system it is still challenging to fill the active materials into the porous 3D current collectors densely and uniformly. Additionally, the complexity of the synthesis of 3D current collectors, the scale-up of 3D current collectors for real application is still a concern, as a practical 3D current collector should be compatible with the downstream manufacturing process. Currently, research on methods for preparing a 3D current collector has made some progress, but a simple and inexpensive method for large-scale production still needs to be defined. Besides, reported methods are complex and require a significant amount of time, which does not apply to mass production. Therefore, future research should develop facile, cheap, and fast preparation methods for 3D current collectors. And the last but not the least concern is the cell design. Whether it is an all 3D solid-state battery or quasi 3D electrodes, the cell with 3D current collectors needs to be designed to protect the porous structure and ensure compact

Table 1
Summary of 3D current collectors and their electrochemical properties used in rechargeable batteries.

Material	Electrode/battery	Synthesis method	Electrochemical performance	Ref.
Ni foam	Cu-Sn/Ni/LIB	CVD/ electrodeposition	500 mAh g^{-1} at 0.2 C	30
Ni foam	C–Si/Ni/LIB	Commercial	300 mAh g^{-1} (100th) at 1.5-0 V/C/15	31
Ni foam	S@Ni/Li-S	Commercial	>810 mAh g^{-1} (50th) at 1.5-2.8 V	32
Ni foam	$Co_3V_2O_8$/Ni/LIB	Commercial	1586.9 mAh g^{-1} (1st) and 1289 mAh g^{-1} (100th) at 0.01-3 V/200 mAh g^{-1}	35
Ni foam	$CuCo_2O_4$/Ni/LIB	Commercial	1700 mAh g^{-1} (100th) at 0.01-3 V/200 mAh g^{-1}	36
Ni foam	$Ni(OH)_2$/RGO/$Ni(OH)_2$/Ni/LIB	Commercial	1662 mAh g^{-1} (2nd) and 1330 mAh g−1 (200th) at 0.01–3.0 V/100 mAh g^{-1}	37
Ni foam	Ni_3S_2/Ni/LIB	Commercial	700 mAh g^{-1} (1st) and 623 mAh g^{-1} (150th) at 0.01–3.0 V/0.1 Ah g^{-1}	38
Ni foam	Fe_3O_4/Ni/C/Ni/LIB	Commercial	1184.5 mAh g^{-1} (1st) and 848.7 mAh g^{-1} (50th) at 0.02–3.0 V/0.3 C	40
Ni foam	ZnO@Ni/LIB	Commercial	731 mAh g^{-1} (1st) and 565 mAh g^{-1} (100th) at 0.02–3.0 V/100 mAh g^{-1}	42
Ni foam	ZnO nanosheets@Ni/LIB	Commercial	1507 mAh g^{-1} (1st) and 1292 mAh g^{-1} (45th) at 0.01–3.0 V/0.2 Ah g^{-1}	43
Ni foam	Co_3O_4 NW/Ni/LIB	Commercial	1327 mAh g^{-1} (1st) and 71.7 % of initial capacity (100th) at 0.01–3.0 V/0.2 Ah g^{-1}	44
Ni foam	Co_3O_4/CuO NW/Ni/LIB	Commercial	1633 mAh g^{-1} (1st) and 1191 mAh g^{-1} (200th) at 0.01–3.0 V/200 mAh g^{-1}	45
Ni foam	NCS/Ni/LIB	Commercial	2563 mAh g^{-1} (1st) and 2081 mAh g^{-1} (100th) at 0.05–3 V/200 mAh g^{-1}	46
Ni foam	ZnO/Ni/LIB	Commercial	1784 mAh g^{-1} (1st) and 402 mAh g^{-1} (100th) at 0.01–3.0 V/200 mAh g^{-1}	48
Ni foam	NiO–$NiCo_2O_4$/Ni/LIB	Commercial	2112 mAh g^{-1} (1st) and 1466 mAh g^{-1} (100th) at 0.01–3.0 V/400 mA g^{-1}	49
Ni foam	Sn/Ni/LIB	Commercial	890 mAh g^{-1} (1st) and 667 mAh g^{-1} (2nd) at 0.02–1.5 V/0.2 A cm^{-2}	50
Ni foam	SnO_2/graphene/Ni/LIB	Commercial	1642 mAh g^{-1} (1st) at 200 mAh g^{-1} and 757 mAh g^{-1} (500th) at 0.01–3.0 V/1 A g^{-1}	51
Ni foam	Li_2TiO_3/Ni/LIB	Commercial	153 mAh g^{-1} (1st) at 200 mAh g^{-1} and 145 mAh g^{-1} (30th) at 0.01–1.0 V/1 mAh g^{-1}	52
C foam	UGF/LFP/LIB	CVD	70 mAh g^{-1} at 2–5 V/1280 mAh g^{-1}	53
C foam	GF–rGO/S/Li-S	CVD	1000 mAh g^{-1} (1st) and 645 mAh g^{-1} (350th) at 2.8–1.5 V/C/5 (1 C = 1675 mAh g^{-1})	54
C foam	UFG-V_2O_5/PEDOT core/shell NBA/LIB	CVD	265 mAh g^{-1} (1st) at 2.0–4.0 V/5 C maintain 98 % after 1000 cycles	56
C foam	S-PDMS/GF/Li-S	CVD	>450 mAh g^{-1} (1000th) at 1.5-2.8 V/6 A g^{-1}	57
C foam	S@ FLG/Li-S	CVD	1143 mAh g^{-1} (1st) at 400 mAh g^{-1} and ~300 mAh g^{-1} (400th) at 1.5–3.0 V/3200 mA g^{-1}	58
C foam	LFP/GF/LIB	CVD	~143 mAh g^{-1} (1st) at 0.8–2.5 V/0.2 C (1 C = 145 mAh g^{-1})	59
C foam	Si/graphene/UGF/LIB	CVD	983 mAh g^{-1} (1st) and 370 mAh g^{-1} (100th) at 0.01–2.2 V/1.5 mA g^{-1}	60
C foam	Ge-QD@NG/NGF/LIB	CVD	1220 mAh g^{-1} (1st) and 1194 mAh g^{-1} (10th) at 0.01–1.5 V/1 C (1 C = 1600 mA g^{-1} for Ge)	61
Cu foam	Sn–Co@3D-Cu/LIB	Electrodeposition	550 mAh g^{-1} (1st) and 108 mAh g^{-1} (50th) at 0.02–1.5 V/50 mA g^{-1}	64
Cu foam	Si@3D-Cu/LIB	Electrodeposition	1000 mAh g^{-1} at 0.01–1.5 V/50 mAh g^{-1}	65
Cu foam	CuO/3D-Cu/LIB	Commercial	1112.3 mAh g^{-1} (1st) and 523.9 mAh g^{-1} (100th) at 0.01–3.0 V/0.5 A g^{-1}	66
Cu foam	CuCl@3D-Cu/LIB	Commercial	197.2 mAh g^{-1} (1000th) at 0.1–3.0 V/10 C	67
Cu foam	Cu2O@3D-Cu/LIB	Commercial	1058.3 mAh g^{-1} (1st) and 385.3 mAh g^{-1} (100th) at 0.01–3.0 V/1.5 C	68
Cu foam	Si/3D-Cu/Ag/LIB	Commercial	1450 mAh g^{-1} (100th) at 0.01–2.0 V/2000 mAh g^{-1}	69
Cu foam	Si/CNFs-3D-Cu/LIB	Commercial	1400 mAh g^{-1} (1^{th}) and 814 mAh g^{-1} (80th) at 0.01–1.20 V/0.5 A g^{-1}	70
Cu foam	TiO_2@C/3D-Cu/LIB	Commercial	394.8 mAh g^{-1} (1^{th}) and 338.6 mAh g^{-1} (200th) at 0.01–3.0 V/1.5 A g^{-1}	71
Cu foam	SnO_2/3D-Cu/LIB	Commercial	~1.6 mAh cm^{-2} (1^{th}) and 1.3 mAh cm^{-2} (50th) a^{t} 0.01-3 V/0.5 mA cm^{-2}	72
Cu foam	$Cu_{0.39}Zn_{0.14}Co_{2.47}O_4$–CuO@CNTs/CF/ LIB	Commercial	227 mAh g^{-1} (1^{th}) and 174 mAh g^{-1} (100th) at 3.0–4.2 V/0.2 A g^{-1}	73
Cu foam	Li@Cu/LIB	Chemical dealloying	136 mAh g^{-1} (30th) at 0.0–1.0 V/0.5 C	25
Cu foam	3D-Cu@Li/LIB	Chemical dealloying	137.5 mAh g^{-1} (1^{th}) at 0.0–1.0 V/1 mAh cm^{-2}, 80 % retention after 150 cycles	78
CuZn foam	Li@3D-CuZn/LIB	Chemical dealloying	220 cycles with 95 % of CE at 0.01–1.5 V/0.05 mAh cm^{-2}	83
Cu foam	Sn@np-Cu/LIB	Chemical dealloying	4.05 mAh cm^{-2} (1st) and s 1.03 mAh cm^{-2} (10th) at 1.5–0.01 V/150 mAh g^{-1}	79
Cu foam	Sn@3D-Cu/LIB	Chemical dealloying	3.67 mAh cm^{-2} (1st) and 1.29 mAh cm^{-2} (30th) at 2–0.01 V/0.5 A cm^{-2}	80
Cu foam	Li@3D-Cu/LIB	Physical dealloying	151 mAh g^{-1} (1st) and 99 % of 1st (15th) at 2.4–4.2 V/0.5 C	84
Cu foam	Li@3D-Cu/LIB	Physical dealloying	147.7 mAh g^{-1} (1st) and 128.8 mAh g^{-1} (300th) at 0–1 V/50 mA g^{-1}	82
Ni foam	$NiC_2O_4 \cdot 2H_2O$@np-Ni/LIB	Hydrothermal	3154 mAh g^{-1} (1st) and 1247 mAh g^{-1} (30th) at 3.0–0.005 V/100 mAh g^{-1}	85
NiCr foam	LFP/NiCr/LIB	Alloying	150 mAh g^{-1} at 2.0–5.0 V/0.2 C	86
Carbon foam	NCF@CNT/S/Li-S	Pyrolysis	1124 mAh g^{-1} (1st) and 903 mAh g^{-1} (100th) at 1.8–3.0 V/0.5 C	92
Carbon foam	TiO_2- NCF/LIB	Pyrolysis	188 mAh g^{-1} (1st) at 1.0–3.0 V/200 mAh g^{-1} and 149 mAh g^{-1} (100th) at 1.0–3.0 V/ 1000 mAh g^{-1}	93
Carbon foam	CF/SnO_2/LIB	Pyrolysis	453 mAh g^{-1} (100th) at 0.1–2.5 V/500 mAh g^{-1}	94
Carbon foam	Ti@CF - Si/LIB	Pyrolysis	1560 mAh g^{-1} (1st) and 861 mAh g^{-1} (100th) at 2.6–4.3 V/1.0 A g^{-1}	95
Carbon fiber	S/DPAN/CNT/Li-S	Pyrolysis	2000 mAh g^{-1} (1st) and 1104 mAh g^{-1} (100th) at 1.0–3.0 V/0.1 C	98
Carbon fiber	CFC - S/PPy/Li-S	Pyrolysis	884 mAh g^{-1} (1st) and 397 mAh g^{-1} (50th) at 1.0–3.0 V/0.5 C	99
Carbon fiber	CNFs/CuNPs/Li/LIB	Pyrolysis	124 mAh g^{-1} (400th) at 3–4.2 V/140 mAh g^{-1}	100
Carbon fiber	VN@NCNF- Li_2S_6/Li-S	Pyrolysis	935 mAh g^{-1} (1st) and 700 mAh g^{-1} (500th) at 1.8–2.8 V/0.2 C	101
Carbon fiber	TiO_2@NCNF-S/Li-S	Pyrolysis	865 mAh g^{-1} (1st) and 786 mAh g^{-1} (200th) at 1.8–2.8 V/0.2 C	102
Carbon fiber	LVP@C/LIB	Pyrolysis	142 mAh g^{-1} (1st) at 3.0–4.8 V/10 C and 123 mAh g^{-1} (500th) at 3.0-4.8 V/1 C	103
Carbon fiber	NanoSi@CFP/LIB	Pyrolysis	1170 mAh g^{-1} (1st) and 1136 mAh g^{-1} (400th) at 0.0–2.0 V/0.5 A g^{-1}	104
Carbon paper	CP@TiO_2-S/Li-S	Pyrolysis	1606 mAh g^{-1} (1st) and 850 mAh g^{-1} (200th) at 1.5–3.0 V/0.5C (1C = 1675 mAh g^{-1})	107
Carbon paper	Si/C/CP/LIB	Pyrolysis	1720 mAh g^{-1} (1st) and 1200 mAh g^{-1} (100th) at 0.02–1.5 V/100 mA g^{-1}	108

Abbreviations: NW - nanowire; NCS - nickel cobalt sulfide; PEDOT - poly(3,4-ethylenedioxythiophene); FLG - few-layered graphene; UGF - ultrathin-graphite foam; Ge-QD@NG/NGF - porous nitrogen-doped graphene foam (NGF) with encapsulated Ge quantum dot@nitrogen-doped graphene yolk-shell nanoarchitecture; np - nanoporous; CNT - multiwalled carbon nanotube; S/PPy - sulfur/polypyrrole; CFC - carbon fiber cloth; VN - vanadium nitride; NCNF - N-doped carbon nanofibers; LVP - $Li_3V_2(PO_4)_3$; CFP - carbon fiber papers; CP - carbon paper.

packaging.

Author contributions

The manuscript was written through contributions of all authors. All authors have given approval to the final version of the manuscript. The authors declare that they have no known competing financial interests or personal relationships that could have appeared to influence the work reported in this paper.

Declaration of competing interest

The authors declare that they have no known competing financial interests or personal relationships that could have appeared to influence the work reported in this paper.

Acknowledgements

This work was supported by the research projects AP08052143 "Development of Wearable Self-Charging Power Unit" and AP09258691 "MXenes based 3D printed energy storage devices" from the Ministry of Education and Science of the Republic of Kazakhstan and the research grants 091019CRP2114 "Three-Dimensional All Solid State Rechargeable Batteries" and 240919FD3914 "Self-Charging Rechargeable Lithium-ion Battery" from Nazarbayev University.

References

[1] J.B. Goodenough, K.S. Park, J. Am. Chem. Soc. 135 (2013) 1167–1176, https://doi.org/10.1021/ja3091438.
[2] L. Kong, H.J. Peng, J.Q. Huang, Q. Zhang, Nano Res. 10 (2017) 4027–4054, https://doi.org/10.1007/s12274-017-1652-x.
[3] H. Abe, M. Kubota, M. Nemoto, Y. Masuda, Y. Tanaka, H. Munakata, K. Kanamura, J. Power Sources 334 (2016) 78–85, https://doi.org/10.1016/j.jpowsour.2016.10.016.
[4] X. Yao, Y. Zhao, Chem 2 (2017) 171–200, https://doi.org/10.1016/j.chempr.2017.01.010.
[5] W. Lu, J.B. Baek, L. Dai, Carbon nanomater, Adv. Energy Syst. Adv. Mater. Synth. Device Appl. (2015) 1–448, https://doi.org/10.1002/9781118980989.
[6] S.T. Myung, K. Amine, Y.K. Sun, J. Mater. Chem. 20 (2010) 7074–7095, https://doi.org/10.1039/c0jm00508h.
[7] P.V. Braun, J. Cho, J.H. Pikul, W.P. King, H. Zhang, Curr. Opin. Solid State Mater. Sci. 16 (2012) 186–198, https://doi.org/10.1016/j.cossms.2012.05.002.
[8] D.Y. Shin, D.H. Park, H.J. Ahn, Appl. Surf. Sci. 475 (2019) 519–523, https://doi.org/10.1016/j.apsusc.2019.01.016.
[9] L. Wang, X. He, J. Li, J. Gao, M. Fang, G. Tian, J. Wang, S. Fan, J. Power Sources 239 (2013) 623–627, https://doi.org/10.1016/j.jpowsour.2013.02.008.
[10] S.W. Kim, K.Y. Cho, J. Electrochem. Sci. Technol. 6 (2015) 1–6.
[11] L. Mai, X. Tian, X. Xu, L. Chang, L. Xu, Chem. Rev. 114 (2014) 11828–11862, https://doi.org/10.1021/cr500177a.
[12] J. Billaud, C. Eames, N. Tapia-Ruiz, M.R. Roberts, A.J. Naylor, A.R. Armstrong, M. S. Islam, P.G. Bruce, Adv. Energy Mater. 7 (2017) 1–9, https://doi.org/10.1002/aenm.201601043.
[13] Z. Wang, X. Zhang, Y. Yan, Y. Zhang, Y. Wang, C. Qin, Z. Bakenov, Nanoporous GeO 2/Cu/Cu 2 O network synthesized by dealloying method for stable Li-ion storage, Electrochim. Acta 300 (2019) 363–372, https://doi.org/10.1016/j.electacta.2019.01.127.
[14] A.H. Whitehead, M. Schreiber, Current collectors for positive electrodes of lithium-based batteries, J. Electrochem. Soc. 152 (2005), A2105, https://doi.org/10.1149/1.2039587.
[15] A.K. Singh, L. Cao, J. Ma, J. Seo, C.E. Bakis, Y. Zhang, M.A. Hickner, C.D. Rahn, Des., J. Sandw. Struct. Mater. 17 (2015) 666–690, https://doi.org/10.1177/1099636215591908.
[16] A.J. Bard, L.R. Faulkner, Fundamentals Appl. (1980), https://doi.org/10.1146/annurev.matsci.30.1.117.
[17] Y.-G. Guo, J.-S. Hu, L.-J. Wan, Adv. Mater. 20 (2008) 2878–2887, https://doi.org/10.1002/adma.200800627.
[18] M. Yamada, T. Watanabe, T. Gunji, J. Wu, F. Matsumoto, Electrochemistry 1 (2020) 124–159, https://doi.org/10.3390/electrochem1020011.
[19] S. Theivaprakasam, G. Girard, P. Howlett, M. Forsyth, S. Mitra, D. MacFarlane, Npj Mater. Degrad. 2 (2018), https://doi.org/10.1038/s41529-018-0033-6.
[20] M. Yao, K. Okuno, T. Iwaki, M. Kato, S. Tanase, K. Emura, T. Sakai, Electrochem. Solid State Lett. 10 (2007) 245–249, https://doi.org/10.1149/1.2776129.
[21] M. Hagen, D. Hanselmann, K. Ahlbrecht, R. Maça, D. Gerber, J. Tübke, Adv. Energy Mater. 5 (2015), https://doi.org/10.1002/aenm.201401986.
[22] Y.L. Kim, Y.K. Sun, S.M. Lee, Electrochim. Acta 53 (2008) 4500–4504, https://doi.org/10.1016/j.electacta.2008.01.050.
[23] T. Ould Ely, D. Kamzabek, D. Chakraborty, Front. Energy Res. 7 (2019), https://doi.org/10.3389/fenrg.2019.00071.
[24] Q. Li, S. Zhu, Y. Lu, Adv. Funct. Mater. 27 (2017) 1–8, https://doi.org/10.1002/adfm.201606422.
[25] Q. Yun, Y.B. He, W. Lv, Y. Zhao, B. Li, F. Kang, Q.H. Yang, Adv. Mater. 28 (2016) 6932–6939, https://doi.org/10.1002/adma.201601409.
[26] K.Y. Song, G.S. Jang, J. Tao, J.H. Lee, S.K. Joo, J. Nanosci. Nanotechnol. 18 (2018) 992–998, https://doi.org/10.1166/jnn.2018.13953.
[27] T. Kodas, Handbook of Chemical Vapor Deposition (CVD), Principles, Technology, and Applications, ByHugh O. Pierson, Noyes, Park Ridge, NJ, 1992, p. 436, https://doi.org/10.1002/adma.19930050522, hardback, $ 68, ISBN 0-8155-1300-3, 1993.
[28] K.L. Choy, Chemical vapour deposition of coatings, Prog. Mater. Sci. 48 (2003) 57–170, https://doi.org/10.1016/S0079-6425(01)00009-3.
[29] O.B. Olurin, D.S. Wilkinson, G.C. Weatherly, V. Paserin, J. Shu, Compos. Sci. Technol. 63 (2003) 2317–2329, https://doi.org/10.1016/S0266-3538(03)00265-3.
[30] V. Poserin, S. Marcuson, J. Shu, D.S. Wilkinson, Adv. Eng. Mater. 6 (2004) 454–459, https://doi.org/10.1002/adem.200405142.
[31] M. Yao, K. Okuno, T. Iwaki, T. Awazu, T. Sakai, J. Power Sources 195 (2010) 2077–2081, https://doi.org/10.1016/j.jpowsour.2009.10.014.
[32] Q. Sa, Y. Wang, J. Power Sources 208 (2012) 46–51, https://doi.org/10.1016/j.jpowsour.2012.02.020.
[33] S.H. Chung, A. Manthiram, Electrochim. Acta 107 (2013) 569–576, https://doi.org/10.1016/j.electacta.2013.06.034.
[34] B. Tolegen, A. Adi, A. Aishova, Z. Bakenov, A. Nurpeissova, Mater. Today Proc. 4 (2017) 4491–4495, https://doi.org/10.1016/j.matpr.2017.04.021.
[35] A. Nurpeissova, A. Adi, A. Aishova, A. Mukanova, S.S. Kim, Z. Bakenov, Mater. Today Energy 16 (2020), 100397, https://doi.org/10.1016/j.mtener.2020.100397.
[36] Y. Li, L. Bin Kong, M.C. Liu, W. Bin Zhang, L. Kang, Ceram. Int. 43 (2017) 1166–1173, https://doi.org/10.1016/j.ceramint.2016.10.058.
[37] Y. Li, M. Liu, S. Hou, P. Wang, X. Pan, M. Xie, Y. Chen, L. Zhao, Appl. Surf. Sci. 458 (2018) 517–522, https://doi.org/10.1016/j.apsusc.2018.07.071.
[38] S. Min, C. Zhao, P. Ju, T. Zhou, H. Gao, Y. Zheng, H. Wang, G. Chen, X. Qian, Z. Guo, J. Power Sources 304 (2016) 311–318, https://doi.org/10.1016/j.jpowsour.2015.11.053.
[39] Z. Zhang, H. Zhao, Q. Xia, J. Allen, Z. Zeng, C. Gao, Z. Li, X. Du, K. Świerczek, Electrochim. Acta 211 (2016) 761–767, https://doi.org/10.1016/j.electacta.2016.06.103.
[40] Z. Hou, C. Shu, J. Long, Electrochim. Acta 290 (2018) 657–665, https://doi.org/10.1016/j.electacta.2018.08.139.
[41] Z. Li, H. Zhao, J. Wang, P. Lv, Z. Zhang, Z. Zeng, Q. Xia, Electrochim. Acta 182 (2015) 398–405, https://doi.org/10.1016/j.electacta.2015.09.086.
[42] H.K. Kang, S.G. Woo, J.H. Kim, S.R. Lee, D.G. Lee, J.S. Yu, J. Power Sources 413 (2019) 467–475, https://doi.org/10.1016/j.jpowsour.2018.12.075.
[43] H. Yang, L. Chang, L. Wang, D. Yin, D. Wang, Y. Cheng, Ionics 26 (2020) 3281–3288, https://doi.org/10.1007/s11581-019-03424-4.
[44] T. Xia, Y. Wang, C. Mai, G. Pan, L. Zhang, W. Zhao, J. Zhang, RSC Adv. 9 (2019) 19253–19260, https://doi.org/10.1039/c9ra03373d.
[45] J. Zheng, B. Zhang, Ceram. Int. 40 (2014) 11377–11380, https://doi.org/10.1016/j.ceramint.2014.02.108.
[46] J. Wang, Q. Zhang, X. Li, D. Xu, Z. Wang, H. Guo, K. Zhang, Nano Energy 6 (2014) 19–26, https://doi.org/10.1016/j.nanoen.2014.02.012.
[47] H.L. Chen, P.S. Wu, J.J. Wu, ACS Sustain. Chem. Eng. 7 (2019) 17100–17106, https://doi.org/10.1021/acssuschemeng.9b03329.
[48] X.Y. Yue, W.W. Wang, Q.C. Wang, J.K. Meng, Z.Q. Zhang, X.J. Wu, X.Q. Yang, Y. N. Zhou, Energy Storage Mater. 14 (2018) 335–344, https://doi.org/10.1016/j.ensm.2018.05.017.
[49] J. Yuan, X. Zhang, C. Chen, Y. Hao, R. Agrawal, C. Wang, W. Li, H. Yu, Y. Yu, X. Zhu, Z. Xiong, Y. Xie, Mater. Lett. 190 (2017) 37–39, https://doi.org/10.1016/j.matlet.2016.12.126.
[50] J. Yuan, S. Gao, W. Lai, S. Zheng, J. Meng, X. Zhang, X. Zhu, H. Yu, X. Li, J. Mater. Sci. Mater. Electron. 30 (2019) 16008–16014, https://doi.org/10.1007/s10854-019-01971-0.
[51] M. Tokur, H. Algul, M. Uysal, T. Cetinkaya, A. Alp, H. Akbulut, Surf. Coating. Technol. 288 (2016) 62–68, https://doi.org/10.1016/j.surfcoat.2016.01.015.
[52] L. Zhan, X. Zhou, J. Luo, X. Ning, Ceram. Int. 45 (2019) 6931–6936, https://doi.org/10.1016/j.ceramint.2018.12.190.
[53] Z. Chen, W. Ren, L. Gao, B. Liu, S. Pei, H.M. Cheng, Nat. Mater. 10 (2011) 424–428, https://doi.org/10.1038/nmat3001.
[54] H. Ji, L. Zhang, M.T. Pettes, H. Li, S. Chen, L. Shi, R. Piner, R.S. Ruof, Nano Lett. 12 (2012) 8–13.
[55] G. Hu, C. Xu, Z. Sun, S. Wang, H.M. Cheng, F. Li, W. Ren, Adv. Mater. 28 (2016) 1603–1609, https://doi.org/10.1002/adma.201504765.
[56] G.H. Lee, J.W. Lee, J.I.L. Choi, S.J. Kim, Y.H. Kim, J.K. Kang, Adv. Funct. Mater. 26 (2016) 5139–5148, https://doi.org/10.1002/adfm.201601355.
[57] D. Chao, X. Xia, J. Liu, Z. Fan, C.F. Ng, J. Lin, H. Zhang, Z.X. Shen, H.J. Fan, Adv. Mater. 26 (2014) 5794–5800, https://doi.org/10.1002/adma.201400719.
[58] G. Zhou, L. Li, C. Ma, S. Wang, Y. Shi, N. Koratkar, W. Ren, F. Li, H.M. Cheng, Nano Energy 11 (2015) 356–365, https://doi.org/10.1016/j.nanoen.2014.11.025.
[59] K. Xi, P.R. Kidambi, R. Chen, C. Gao, X. Peng, C. Ducati, S. Hofmann, Nanoscale 6 (2014) 5746–5753, https://doi.org/10.1039/c4nr00326h.
[60] N. Li, Z. Chen, W. Ren, F. Li, H.M. Cheng, Proc. Natl. Acad. Sci. U. S. A 109 (2012) 17360–17365, https://doi.org/10.1073/pnas.1210072109.

[61] J. Ji, H. Ji, L.L. Zhang, X. Zhao, X. Bai, X. Fan, F. Zhang, R.S. Ruoff, Adv. Mater. 25 (2013) 4673–4677, https://doi.org/10.1002/adma.201301530.
[62] R. Mo, D. Rooney, K. Sun, H.Y. Yang, Nat. Commun. 8 (2017), https://doi.org/10.1038/ncomms13949.
[63] A.M.F. Dehkharghani, M. Divandari, Trans. Inst. Met. Finish. 93 (2015) 186–189, https://doi.org/10.1179/0020296715Z.000000000248.
[64] H.C. Shin, M. Liu, Chem. Mater. 16 (2004) 5460–5464, https://doi.org/10.1021/cm048887b.
[65] X.Y. Fan, F.S. Ke, G.Z. Wei, L. Huang, S.G. Sun, J. Alloys Compd. 476 (2009) 70–73, https://doi.org/10.1016/j.jallcom.2008.09.030.
[66] F. Dogan, L.D. Sanjeewa, S.J. Hwu, J.T. Vaughey, Solid State Ionics 288 (2016) 204–206, https://doi.org/10.1016/j.ssi.2016.02.001.
[67] W. Yang, J. Wang, W. Ma, C. Dong, G. Cheng, Z. Zhang, J. Power Sources 333 (2016) 88–98, https://doi.org/10.1016/j.jpowsour.2016.09.154.
[68] S. Liu, H. Hou, X. Liu, W. Hu, C. Yan, J. Duan, R. Meng, Ceram. Int. 42 (2016) 8310–8315, https://doi.org/10.1016/j.ceramint.2016.02.044.
[69] W. Chen, W. Zhang, L. Chen, L. Zeng, M. Wei, J. Alloys Compd. 723 (2017) 172–178, https://doi.org/10.1016/j.jallcom.2017.06.153.
[70] L. Zhou, W. Ma, L. Yang, L. shao, J. Zhou, C. Yang, X. Liu, X. Xi, Mater. Lett. 244 (2019) 199–202, https://doi.org/10.1016/j.matlet.2019.02.013.
[71] X. Tian, G. Li, L. Meng, W. Tian, X. Gu, Y. Ding, R. Zhang, X. Jia, Y. Qin, Mater. Lett. 268 (2020), 127572, https://doi.org/10.1016/j.matlet.2020.127572.
[72] C. sheng An, B. Zhang, L. bo Tang, B. Xiao, Z. jiang He, J. chao Zheng, Ceram. Int. 45 (2019) 13144–13149, https://doi.org/10.1016/j.ceramint.2019.03.249.
[73] J.H. Um, H. Kim, Y.H. Cho, W.S. Yoon, J. Electrochem. Sci. Technol. 11 (2020) 92–98, https://doi.org/10.33961/jecst.2019.00493.
[74] L. Lu, J.T.M. De Hosson, Y. Pei, Carbon N. Y. 144 (2019) 713–723, https://doi.org/10.1016/j.carbon.2018.12.103.
[75] Y. Sun, Y. Ren, K. Yang, Mater. Lett. 165 (2016) 1–4, https://doi.org/10.1016/j.matlet.2015.11.102.
[76] J. Erlebacher, M.J. Aziz, A. Karma, N. Dimitrov, K. Sieradzki, Nature 410 (2001) 450–453, https://doi.org/10.1038/35068529.
[77] Y. Shi, Z. Wang, H. Gao, J. Niu, W. Ma, J. Qin, Z. Peng, Z. Zhang, J. Mater. Chem. 7 (2019) 1092–1098, https://doi.org/10.1039/c8ta09384a.
[78] D. Zhang, A. Dai, M. Wu, K. Shen, T. Xiao, G. Hou, J. Lu, Y. Tang, ACS Energy Lett. 5 (2020) 180–186, https://doi.org/10.1021/acsenergylett.9b01987.
[79] S. Zhang, Y. Xing, T. Jiang, Z. Du, F. Li, L. He, W. Liu, J. Power Sources 196 (2011) 6915–6919, https://doi.org/10.1016/j.jpowsour.2010.12.021.
[80] Z. Luo, J.C. Xu, B. Yuan, H. Li, R.Z. Hu, L.C. Yang, Y. Gao, M. Zhu, Mater. Lett. 213 (2018) 189–192, https://doi.org/10.1016/j.matlet.2017.11.089.
[81] J.R. Hayes, A.M. Hodge, J. Biener, A.V. Hamza, K. Sieradzki, J. Mater. Res. 21 (2006) 2611–2616, https://doi.org/10.1557/jmr.2006.0322.
[82] Y. An, H. Fei, G. Zeng, X. Xu, L. Ci, B. Xi, S. Xiong, J. Feng, Y. Qian, Nano Energy 47 (2018) 503–511, https://doi.org/10.1016/j.nanoen.2018.03.036.
[83] H. Liu, E. Wang, Q. Zhang, Y. Ren, X. Guo, L. Wang, G. Li, H. Yu, Energy Storage Mater. 17 (2019) 253–259, https://doi.org/10.1016/j.ensm.2018.07.010.
[84] L. Lu, P. Andela, J.T.M. De Hosson, Y. Pei, ACS Appl. Nano Mater. 1 (2018) 2206–2218, https://doi.org/10.1021/acsanm.8b00284.
[85] M. Yao, K. Okuno, T. Iwaki, M. Kato, S. Tanase, K. Emura, J. Power Sources 173 (2007) 545–549, https://doi.org/10.1016/j.jpowsour.2007.08.014.
[86] G.F. Yang, S.K. Joo, Electrochim. Acta 170 (2015) 263–268, https://doi.org/10.1016/j.electacta.2015.04.119.
[87] K.Y. Song, G.S. Jang, J. Tao, J.H. Lee, S.K. Joo, J. Electrochem. Soc. 163 (2016) A2981–A2987, https://doi.org/10.1149/2.0581614jes.
[88] G.F. Yang, K.Y. Song, S.K. Joo, RSC Adv. 5 (2015) 16702–16706, https://doi.org/10.1039/c4ra14485f.
[89] K.Y. Song, S.K. Joo, Mater. Res. Bull. 94 (2017) 328–334, https://doi.org/10.1016/j.materresbull.2017.06.026.
[90] Z. Cao, J. Zhang, Y. Ding, Y. Li, M. Shi, H. Yue, Y. Qiao, Y. Yin, S. Yang, J. Mater. Chem. 4 (2016) 8636–8644, https://doi.org/10.1039/c6ta01855f.
[91] S. Chu, Y. Zhong, R. Cai, Z. Zhang, S. Wei, Z. Shao, Small 12 (2016) 6724–6734, https://doi.org/10.1002/smll.201602179.
[92] Y. Ma, H.D. Asfaw, K. Edström, J. Power Sources 294 (2015) 208–215, https://doi.org/10.1016/j.jpowsour.2015.06.060.
[93] Z. Liu, S. Bai, B. Liu, P. Guo, M. Lv, D. Liu, D. He, J. Mater. Chem. 5 (2017) 13168–13175, https://doi.org/10.1039/c7ta03576d.
[94] J. Pusch, B. Wohlmann, Carbon fibers, Elsevier Ltd., 2018, https://doi.org/10.1016/B978-0-08-102228-3.00002-5.
[95] H. Chen, Lignocellulose Biorefinery Feedstock Engineering, 2015, https://doi.org/10.1016/b978-0-08-100135-6.00003-x.
[96] Y. Zhang, Z. Bakenov, Y. Zhao, A. Konarov, Q. Wang, P. Chen, Ionics 20 (2014) 803–808, https://doi.org/10.1007/s11581-013-1042-7.
[97] W. Jia, T. Chen, Y. Wang, S. Qu, Z. Yao, Y. Liu, Y. Yin, W. Zou, F. Zhou, J. Li, Electrochim. Acta 309 (2019) 460–468, https://doi.org/10.1016/j.electacta.2019.04.054.
[98] S. Kalybekkyzy, A. Mentbayeva, Y. Yerkinbekova, N. Baikalov, M.V. Kahraman, Z. Bakenov, Nanomaterials 10 (2020) 1–13, https://doi.org/10.3390/nano10040745.
[99] C. Shang, B. Wei, X. Zhang, L. Shui, X. Wang, G. Zhou, Mater. Lett. 236 (2019) 240–243, https://doi.org/10.1016/j.matlet.2018.10.106.
[100] X. Zhang, Z. Chen, L. Shui, C. Shang, X. Wang, G. Zhou, Nanoscale Adv. 1 (2019) 527–531, https://doi.org/10.1039/c8na00160j.
[101] L.C. Zhang, C.L. Yang, Y.F. Jiang, F. Teng, C.X. Ding, Y. Yu, Z.Y. Wen, C.H. Chen, Electrochim. Acta 114 (2013) 347–351, https://doi.org/10.1016/j.electacta.2013.10.016.
[102] Q. Bao, J. Lee, J.G. Duh, Building 3D porous, Mater. Lett. 202 (2017) 28–31, https://doi.org/10.1016/j.matlet.2017.05.081.
[103] H. Zhang, J. Yang, H. Hou, S. Chen, H. Yao, Sci. Rep. 7 (2017) 1–9, https://doi.org/10.1038/s41598-017-07345-y.
[104] Z. Zhang, Q. Li, K. Zhang, W. Chen, Y. Lai, J. Li, J. Power Sources 290 (2015) 159–167, https://doi.org/10.1016/j.jpowsour.2015.05.010.
[105] Q. Si, M. Matsui, T. Horiba, O. Yamamoto, Y. Takeda, N. Seki, N. Imanishi, J. Power Sources 241 (2013) 744–750, https://doi.org/10.1016/j.jpowsour.2013.05.090.